

Evolution of Skyrmion Crystals in $\text{Fe}_{0.5}\text{Co}_{0.5}\text{Si}$ -Like Quasi-Two-Dimensional Ferromagnets Driven by External Magnetic Field and Temperature

Zhaosen Liu^{a,b1}, Tiantian Huan^b, Hou Ian^{b,c2}

Abstract

Magnetic skyrmions have attracted great research interest in recent years due to their exotic physical properties, scientific merit and potential applications in modern technology. Here, we apply a quantum computational method to investigate the spin configurations of $\text{Fe}_{0.5}\text{Co}_{0.5}\text{Si}$ -like quasi-two-dimensional ferromagnetic system with co-existence of Dzyaloshinsky-Moriya and Heisenberg exchange interactions. We find that within a weak magnetic field perpendicular to the film plane, skyrmion crystal (SkX) of hexagonal-close-packed pattern can be induced, the spin configurations evolve with applied magnetic field and temperature. This quantum model, if scaled, is able to qualitatively reproduce the experimental results of SkX with long periodicity. Especially, when the skyrmion size is around a few nano-meters in diameter, *or more general, when the characteristic length of the material approaches the lattice scale*, the quantum model is expected to be more accurate than the classical ones.

Keywords: Skyrmion Crystal, Dzyaloshinsky-Moriya Interaction, Quantized Simulation Model

¹Email: liuzhsnj@yahoo.com

²Email: houian@umac.mo

1. Introduction

Skyrmions, a novel type of topological magnetic structures observed in solids, have attracted intensive research interest in recent years [1, 2, 3, 4]. The concept of skyrmion was originally introduced in nuclear physics to describe a localized, particle-like configuration in field theory about half century ago [5]. However, these topological structures were lately predicted to exist in magnetic materials based on micromagnetic model [6, 7], and experimentally observed in bulk materials, such as MnSi with the B20 crystal structure [8, 9], $\text{Fe}_{1-x}\text{Co}_x\text{Si}$ and FeGe thin films [10, 11], multi-layer systems [12, 13, 14, 15, 16, 17], as well as insulating magnet Cu_2OSeO_3 [18]. Magnetic skyrmion crystal (SkX) textures are mainly induced by the Dzyaloshinsky-Moriya interaction (DMI) [19, 20]. This chiral interaction exists in the systems with broken structural inversion symmetry, and is present at the surfaces of thin films or the interfaces of multi-layers. Since transition-metal interfaces are essential in spintronic devices, the discovery of SkX on these interfaces [14, 15, 16] has aroused great research interest in using them as novel data-storage device concepts [21, 22].

In three-dimensional (3D) materials, SkX is usually stable in a rather narrow T -region immediately below the transition temperature as observed in neutron scattering experiment conducted on MnSi bulk magnet [9]. However in two-dimensional (2D) systems, SkX can exist over a wide temperature region [11, 23]. For instance, using Lorentz transmission electron microscopy, Yu et al. observed that when $\text{Fe}_{0.5}\text{Co}_{0.5}\text{Si}$ thin film is placed in external magnetic fields, the SkX appears and persists down to almost zero temperature [10]. These skyrmions crystalize in the hexagonal-close-packed (HCP) pattern with a periodicity of about 90 nm.

So far, various descriptions for magnetic skyrmions have been proposed. Most of them include the notion of topology as defined in micromagnetics where the continuous model is applied. There, a magnetic skyrmion can be described with a non-zero integer value of the topological index, referred to as topological charge, or winding number. The topological charge of this spin

texture can be expressed as

$$Q = \frac{1}{4\pi} \int \int \vec{m} \cdot (\partial_x \vec{m} \times \partial_y \vec{m}) dx dy . \quad (1)$$

where \vec{m} is a unit vector specifying the direction of the local magnetic moment, and the integral is taken over the space occupied by the skyrmion.

However, we must bear in mind that the concept of topology can only be rigorously applied in continuous models to infer the stable spin structures [24]. At a size scale less than a few nanometers, or more general, *as the spin-spin correlation length of the material approaches the unit cell scale*, the spin textures of magnetic materials become noncontinuous due to the discretization of the atomic lattice. For instances, the skyrmions formed at interfaces are often a few nanometers in diameter [14, 17, 25, 26]. The real spin structures of these skyrmions naturally differ from those derived from the continuous model based on classical physics.

For the above reasons, we carry out simulations here for a $\text{Fe}_{0.5}\text{Co}_{0.5}\text{Si}$ -like thin film by means of a quantum computational method which we develop in recent years [27, 28, 29, 30, 31, 32, 33]. Following the similar methodology [10], we model the thin film as a 2D magnetic monolayer, and impose the periodic boundary conditions to mimic the quasi-infinite size of the system. In brief, the phenomena observed in our simulations can be summarized as below: In the absence of external magnetic field, the helical texture is the ground state. *When* a weak magnetic field is applied normal to the monolayer, SkX textures of hexagonal-closely-packed (HCP) pattern are induced [10], and the periodic distances for the helical and SkX states agree roughly with the theoretical values [10, 34]. As the field strength is enhanced and temperature changes, the SkX textures can be rotated or/and deformed, and their periodic distances increases. When the external field is sufficiently strong, a skyrmion plus bimeron phase appears, which *still looks* symmetric geometrically. Within further increased external magnetic field, the magnetic system finally becomes ferromagnetic as expected. Very interestingly, the calculated topological charge density for every SkX also forms period-

ical and symmetric lattice which is almost identical to the corresponding magnetic SkX, demonstrating the correctness of our simulations. This quantum model, when scaled, is able to qualitatively reproduce the experimental results for SkX of large spacing distance. On the other hand, when the skyrmion size is around a few nano-meters in diameter, or more general, *as the spin-spin correlation length of the material is in the scale of lattice constant*, the quantized discrete model is expected to be more accurate than the classical ones.

2. The Quantum Computational Method and Related Theory

To simplify the model, a quasi-2D system like $\text{Fe}_{0.5}\text{Co}_{0.5}\text{Si}$ thin film can be modelled as a monolayer ferromagnet with the square crystal structure [10], and its Hamiltonian be expressed as

$$\begin{aligned} \mathcal{H} = & -\frac{1}{2} \sum_{\langle i,j \rangle} \left[\mathcal{J}_{ij} \vec{S}_i \cdot \vec{S}_j - D_{ij} \vec{r}_{ij} \cdot (\vec{S}_i \times \vec{S}_j) \right] \\ & - K_A \sum_i \left(\vec{S}_i \cdot \hat{n} \right)^2 - \mu_B g_S \vec{B} \cdot \sum_i \vec{S}_i . \end{aligned} \quad (2)$$

Here, the first two terms represent the Heisenberg exchange and DM interactions with the strengths of \mathcal{J}_{ij} and D_{ij} between a pair of spins at the i - and j -th lattice sites, respectively, and $\langle ij \rangle$ means that these interactions are limited between the nearest neighboring spins; the third term stands for the uniaxial anisotropy assumed to be perpendicular to the monolayer plane, and the last one denotes the Zeeman energy of the 2D system within an applied magnetic field.

The quantum computational method employed in the present work has been described in details in our published papers [27, 28, 29, 30, 31, 32, 33]. So the spins appearing in the above Hamiltonian are quantum operators instead of classical vectors, and all physical quantities are calculated with quantum formulas. In the Heisenberg representation, when $S = 1$ for example as it is assumed in our simulations, the matrices of the three spin components are:

$$S_x = \frac{1}{2} \begin{pmatrix} 0 & \sqrt{2} & 0 \\ \sqrt{2} & 0 & \sqrt{2} \\ 0 & \sqrt{2} & 0 \end{pmatrix}, \quad S_y = \frac{1}{2i} \begin{pmatrix} 0 & \sqrt{2} & 0 \\ -\sqrt{2} & 0 & -\sqrt{2} \\ 0 & \sqrt{2} & 0 \end{pmatrix}, \quad (3)$$

$$S_z = \begin{pmatrix} 1 & 0 & 0 \\ 0 & 0 & 0 \\ 0 & 0 & -1 \end{pmatrix},$$

respectively.

In light of molecular field theory, the i -th spin is considered to be under the interaction of an effective magnetic field \mathbf{B}_i^M generated by the neighboring magnetic moments. As a result, if the lattice chosen for simulations consist of N spins, the Hamiltonian of the whole magnetic system shown above can be decomposed into N coupled Hamiltonians. Each of them is for a spin, and that for the i -th spin is given by

$$\begin{aligned} \mathcal{H}_i = & - \sum_{\langle i,j \rangle} \left[\mathcal{J}_{ij} \vec{S}_i \cdot \langle \vec{S}_j \rangle - D_{ij} \vec{r}_{ij} \cdot (\vec{S}_i \times \langle \vec{S}_j \rangle) \right] \\ & - K_A \sum_i \left(\vec{S}_i \cdot \hat{n} \right)^2 - \mu_B g_S \vec{B} \cdot \sum_i \vec{S}_i. \end{aligned} \quad (4)$$

This Hamiltonian of a single-spin can be easily diagonalized, and the thermal average of any physical variable A at temperature T can be calculated with

$$\langle A \rangle = \frac{\text{Tr} \left[\hat{A} \exp(\beta \mathcal{H}_i) \right]}{\text{Tr} \left[\exp(\beta \mathcal{H}_i) \right]}, \quad (5)$$

where $\beta = -1/k_B T$.

All of our recent simulations are started from a random magnetic configuration above the transition temperature, then carried out stepwise down to very low temperatures with a reducing temperature step $\Delta T < 0$. This trick is very important, since at high temperatures, the effective magnetic field is relatively weak, the thermal interaction is strong enough to help the spins overcome the energy barriers, so that the code can avoid being trapped in local energy minima, and finally converge down to correct equilibrium states spontaneously. Obviously, for this purpose, $|\Delta T|$ cannot be too large.

At a given temperature, the spins are selected one by one successively to evaluate their thermally averaged values. After all spins in the sample have been visited once, an iteration is completed. The iterations are repeated in

a self-consistent manner. When the ratio $(|\langle \vec{S}'_i \rangle - \langle \vec{S}_i \rangle|)/|\langle \vec{S}_i \rangle|$ between two successive iterations for every spin in the lattice is less than a very small given value τ_0 , convergency is considered to be reached.

The periodical length λ_0 of the SkX observed in the $\text{Fe}_{0.5}\text{Co}_{0.5}\text{Si}$ film plane is around 90 nm [10], and the lattice constant a is about 0.45 nm [35]. Thus, the nearest pair of skyrmions are about $200 a$ apart. In order to display the calculated SkX texture for the $\text{Fe}_{0.5}\text{Co}_{0.5}\text{Si}$ film, the spin wavelength λ was assigned to 10 by Yu et al. in their Monte Carlo simulations [10]. In this scaled model, λ is measured in the unit of the side-length of a grid, and each grid contains $n \times n$ spins where $n = \lambda_0/(\lambda a)$ if both λ_0/a and λ are much larger than 1 [36]. Moreover, the periodic distance of the chiral texture can be determined by the relative strengths of Heisenberg exchange and DM interactions [10],

$$\tan\left(\frac{2\pi}{\lambda}\right) = \frac{D}{\sqrt{2}\mathcal{J}}. \quad (6)$$

So, once λ is given, the ratio D/\mathcal{J} can be estimated with this formula.

For a discrete spin model, the winding number density of a skyrmion at the i -th site can be expressed as

$$\rho_i = \frac{1}{16\pi} \vec{S}_i \cdot \left[(\vec{S}_{i+\hat{x}} - \vec{S}_{i-\hat{x}}) \times (\vec{S}_{i+\hat{y}} - \vec{S}_{i-\hat{y}}) \right]. \quad (7)$$

Here an additional prefactor $1/4$ has been *introduced*, since the spacial distances between the spin pair $(\vec{S}_{i+\hat{x}}, \vec{S}_{i-\hat{x}})$ in the x -direction, and another pair $(\vec{S}_{i+\hat{y}}, \vec{S}_{i-\hat{y}})$ in the y -direction, are both equal to $2a$. Moreover, all spins must be normalized before being inserted to this formula. Afterwards, the averaged winding number per skyrmion can be estimated by dividing the sum over the lattice, $\sum_i \rho_i$, with the total number of skyrmions observed in the lattice. To check the correctness of above formula, the winding numbers have also been calculated with a formula employed by previous authors [37], which gives the same results.

On the other hand, the helicity of a chiral spin texture is defined as [37, 38]

$$\gamma = \frac{1}{N} \sum_i \left(\vec{S}_i \times \vec{S}_{i+\hat{x}} \cdot \hat{x} + \vec{S}_i \times \vec{S}_{i+\hat{y}} \cdot \hat{y} \right). \quad (8)$$

This quantity is attributed to the relativistic spin-orbital coupling, its sign and the magnitude reflect the swirling direction (right-handed or left-handed), and degree of the chirality.

3. Computational Results

When the spin wavelength λ is assigned to 10, the ratio D/\mathcal{J} is determined to be 1.027 from Eq.(6). This value is used in all our simulations that are performed on a 30×30 square lattice, and the periodical boundary conditions are imposed to mimic the quasi-infinity of the 2D magnetic system. For simplicity, we further assign $\mathcal{J}/k_B = 1$ K. That is, all physical quantities are scaled with the Heisenberg exchange strength \mathcal{J} and k_B .

3.1. The Ground Helical State in the Absence of External Magnetic Field

We notice from our calculated results that, in the absence of external magnetic field, the helical texture is spontaneously formed below the transition temperature, $T_M = 3.3 \mathcal{J}$. In Figure 1, the xy component and z -contour of the calculated spin structure are both projected onto the film plane. It is

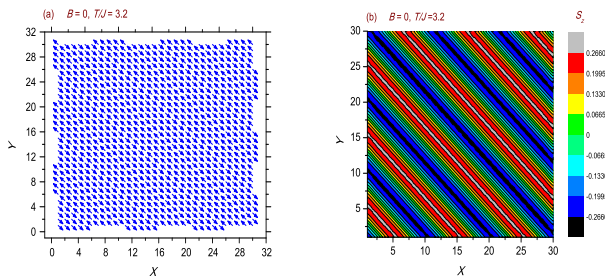


Figure 1. The xy texture (a) and z -contour (b) of the helical spin structure calculated at $T/\mathcal{J} = 3.2$ in the absence of external magnetic field.

interesting to find there that the periodical lengths in the x and y directions of the helix state are all equal to 10 in the unit of grid side length as theoretically predicted. In every spatial period, there exist two spin strips which are anti-parallel in the $[-110]$ direction on the xy -plane, and across each period,

the z -components of the spins change gradually from the minimum with the most negative value to the maximum, then falls down gradually. This helical texture remains unchanged down to almost zero temperature, but the magnitudes of all three components increase with decreasing temperature as expected.

3.2. Initial SkX Textures Induced by a Weak External Magnetic Field

When an external magnetic field is applied perpendicular to the monolayer plane, the helical structure persists until the field is increased to 0.1 Tesla. However, within the magnetic field of this strength, magnetic SkX

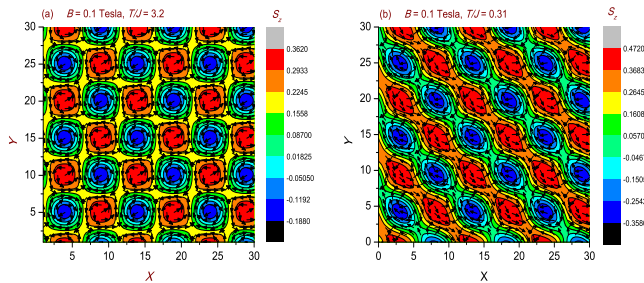


Figure 2. The SkX textures calculated at (a) $T/\mathcal{J} = 3.2$, and (b) $T/\mathcal{J} = 3.1$ in an external magnetic field of 0.1 T applied normal to the monolayer plane.

can be induced at $T/\mathcal{J} = 3.2$, which is immediately below the ferromagnetic phase, as displayed in Figure 2(a). There, 18 skyrmions (printed in blue) are observed on the monolayer plane in a pattern of hexagonal-close-packed (HCP) crystal structure, and they are all separated by shallow vortices (displayed in red). The two sides of such a hexagon are parallel with the x -axis, so it is referred as 'regular' to distinguish it from those rotated and deformed hexagons. However, the external magnetic field is now too weak to stabilize the SkX structure. When temperature falls down to $T/\mathcal{J} = 0.31$, the skyrmions and vortices are all deformed, they are elongated in the $[-110]$ direction, but the chiral spin texture still keeps the regular HCP pattern as shown in Figure 2(b). As the temperature drops further, the SkX texture disappears, being replaced by the helical structure afterwards. *Hou et*

al. have reported the similar phenomenon before [39]. In their Monte Carlo simulations done for a 2D chiral magnet, a surprising upturn of the topological charge was identified at high temperatures. They attributed this upturn to spin fluctuations, that is, the topology was believed to be thermally induced.

3.3. Typical SkX State Induced by Moderate External Magnetic Field

As the external magnetic field is further increased, a stable SkX phase appears over a broad temperature range. For instance, when $B_z = 0.11$ T, SkX is observed in the low temperature region $T/\mathcal{J} \leq 3.2$. Figure 3(a,b) show the SkX textures calculated at $T/\mathcal{J} = 3.2$ and 0.1 respectively within this field. There, every skyrmion is surrounded by four non-fully developed

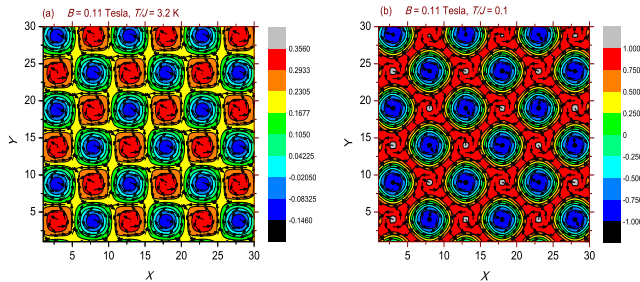


Figure 3. The SkX textures calculated at (a) $T/\mathcal{J} = 3.2$, and (b) $T/\mathcal{J} = 0.1$, within an external magnetic field of 0.11 T applied perpendicular to the monolayer plane.

vortices. Since D is positive, these two sorts of spin textures are both right-handed. They appear alternatively in the lattice plane. All skyrmions curl clockwise, while the vortices swirl anti-clockwise, so as to minimize the total (free) energy of the whole system.

However, in Ref.[10], no surrounding vortices were observed in experimental results and classical Monte Carlo (CMC) simulations. The reasons are given below. To simulate the $Fe_{0.5}Co_{0.5}Si$ -Like 2D system, a scaled model is used here. In this model, one spin represent several hundreds of lattice sites. Thus, vortices curling in the opposite direction must appear to reduce the sudden energy increase caused by the closely packed skyrmions. However,

in real $Fe_{0.5}Co_{0.5}Si$ film, the skyrmions are actually quite large, so the spins can change their directions continuously, thus much smaller or no surrounding vortices are required for the spin texture to relax. On the other hand, in the interstitial areas between the skyrmions, the spins have been considerably rotated by the external magnetic field to the out-of-plane direction, whereas the on-plane components are greatly reduced. Consequently, even the vortices appear in the interstitial areas, they are hardly to be observed in experiments. In contrast, before our simulated spin textures are plotted, the on-plane components of all spins have been normalized, so that the vortices can be easily seen. In Figure 1(b) of Ref.[10], we can see that interstitial areas between the skyrmions are quite large. However, the vortices are missing in these areas. The SkX shown there was obtained in their CMC simulations. We guess that the authors did not do the normalization as we do here.

As expected, though the external magnetic field is applied along the z -axis, the spins inside the skyrmion cores align in the opposite direction. *The increase in total energy incurred by these spins are offset by the surrounding vortices, where the spins have been greatly rotated by the external field toward its orientation.*

Figure 2(a) and Figure 3(a) are obtained at the same temperature, they look very similar at the first glance. However, the vortices and skyrmions have actually exchanged their positions within external magnetic field of different strengths. Moreover, by comparing Figure 3(a) and (b), it is observed that as temperature drops down, the cores of skyrmions expand, but those of the vortices shrink spatially. This rule in general holds in all later cases.

3.4. Vortex Lattice and SkX Formed at $B_z = 0.13$ T

When $B_z = 0.13$ T, an extremely shallow vortex lattice is observed at $T/\mathcal{J} = 3.2$ immediately below the transition temperature as displayed in Figure 4(a). The xy projection of this chiral lattice pattern looks similar to that depicted in Figure 2(a): 18 vortices curl clockwise, other 18 vortices swirl anti-clockwise, and the two sets of vortices appear alternatively on the xy -plane. It can be inferred that such shallow vortical lattices may also be

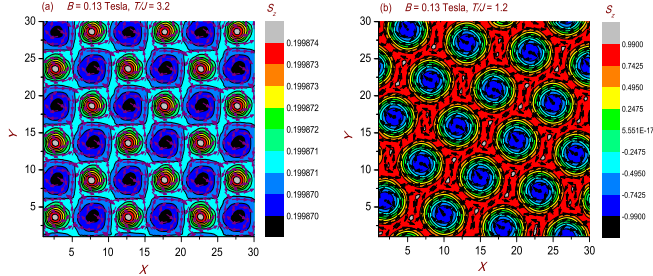


Figure 4. The (a) vortex lattice at $T/\mathcal{J} = 3.2$, and (b) SkX texture at $T/\mathcal{J} = 1.2$, induced by external magnetic field of 0.13 T perpendicular to the monolayer plane.

induced immediately below FM phase by external magnetic field of other strengths, but they are easily destroyed by thermal disturbance, thus can hardly be observed in experiments. When T/\mathcal{J} drops to 3.1, the regular HCP SkX appears, and maintains until $T/\mathcal{J} = 1.3$ over a wide temperature range. While $T/\mathcal{J} \leq 1.2$, the SkX is found to be rotated clockwise for 6° by the effective magnetic field. However, the whole spin structure still keeps HCP pattern as depicted in Figure 4(b).

The spin texture rotation just described above seems very strange, readers may wonder what are the reasons behind. Firstly, the self-consistent algorithm has been implemented into our computing program, so the code can converge spontaneously to the equilibrium states. That is, all spin textures presented in the paper are self-organized, the rotations can not be phantom simply caused by artificial intervention.

Such phenomena will be observed in following figures as well. Theoretically speaking, as temperature or/and the strength of magnetic field vary, not only the magnitudes, but also the orientations of all spins change correspondingly. Since the spins in the system are correlated directly or indirectly, the process may inevitably give rise to spin texture rotation to fit new magnetic configuration. On the other hand, we will see latterly that enhanced magnetic field usually leads to enlarged periodicity. This may also result in SkX rotation so that the spins can adjust themselves to meet the requirements of the

new symmetry and fit the periodical boundary conditions.

3.5. Evolution of SkX Texture Driven by Enhanced External Magnetic Field

At $B_z = 0.15$ T, the same phenomena just described are observed once again. In the temperature range $3.2 > T/\mathcal{J} > 1.9$, the spin texture is a SkX of regular HCP pattern. However, as temperature falls below $T/\mathcal{J} = 1.9$, the SkX texture is not only rotated, but also deformed as shown in Figure 5(a).

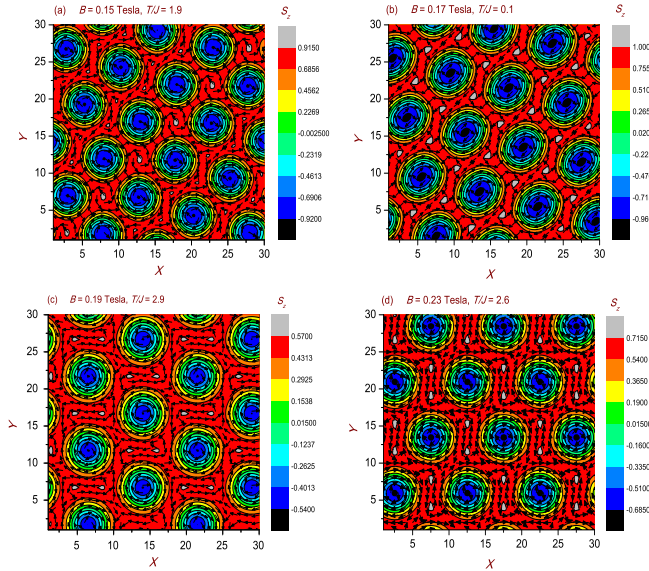


Figure 5. The skyrmion lattices simulated when (a) $B = 0.15$ T, $T/\mathcal{J} = 1.9$, (b) $B = 0.17$ T, $T/\mathcal{J} = 0.1$, (c) $B = 0.19$ T, $T/\mathcal{J} = 2.9$, and (d) $B = 0.23$ T, $T/\mathcal{J} = 2.6$, respectively.

As B_z is increased to 0.17 T, the SkX is rotated by the effective magnetic field once it is formed immediately below the polarized FM phase, and this chiral texture persists from $T/\mathcal{J} = 3.0$ down to very low temperature as shown in Figure 5(b). Now, the HCP SkX pattern is not deformed, however, every skyrmion has been considerably enlarged, and the total number of skyrmions N_s reduced to 15.

As depicted in Figure 5(c), when B_z reaches 0.19 T, the SkX texture has been rotated clockwise further, and the total skyrmion number N_s reduced to 12 in a wide temperature below $T/\mathcal{J} = 2.9$.

Very interestingly, when B_z is increased to, for examples, 0.23, 0.25 and 0.27 T, the spin textures are found to re-assume the regular HCP SkX pattern in the low temperature range as displayed in Figure 5(d), and the total skyrmion numbers are equal to 12 in all these cases.

3.6. Skyrmions Plus Bimerons Texture Formed in the Transition Field

The SkX texture can be maintained until the external magnetic field is increased up to the critical value $B_z^c = 0.28$ T. At $T/\mathcal{J} = 2.4$, which is just below the FM phase, the total skyrmion number N_s is reduced to 8, but the skyrmions are still distributed in the regular HCP pattern as seen in Figure 6(a).

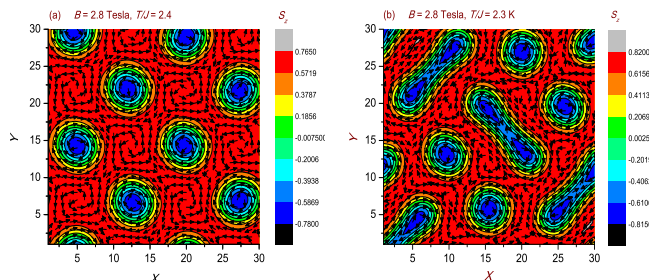


Figure 6. When $B_z = 0.28$ T, (a) SkX, and (b) bimeron textures, are formed at $T/\mathcal{J} = 2.4$ and $T/\mathcal{J} \leq 2.3$, respectively.

Within the external magnetic field of this strength, as temperature drops to the range $T/\mathcal{J} \leq 2.3$, a helix plus SkX texture emerges on the monolayer as shown in Figure 6(b). These helical strips are of finite lengths. They are called as bimerons, and expected to arise above the ground helical strip states when the external magnetic field is sufficiently strong [10, 40, 41]. A bimeron has two half-skyrmions at its two ends, they are connected by a rectangular strip domain. Each of the half-skyrmions bears opposite half skyrmion in the continuous model [40, 41]. The spin structures of the full skyrmions and

bimerons shown in the figure are all right-handed. They are separated by considerably deformed and non-fully developed anti-clockwise vortices, so as to minimize the total energy of the whole magnetic system.

3.7. Finite Helical Strips and Sparse Skyrmions Induced in Strong Magnetic Field

When $B_z = 0.29$ T and $T/\mathcal{J} \leq 2.3$, six helical strips are observed. They are all parallel with $[110]$. Four of these strips terminate inside the 30×30 lattice, and each of them has a half-skyrmion at its one end. So we can speculate that all the strips are finitely long, so they are actually bimerons. The ending half skyrmions are all right-handed, so are the rectangular parts of the strips since $D > 0$. In comparison with those shown in Figure 6(b), these strips are much longer. This effect becomes more evident when B_z is increased to 0.30 T: the helical strips look much longer along the diagonal of the square lattice. Moreover, in the low temperature region $T/\mathcal{J} \leq 2$, the periodical distances between the strips become 10 in the x -direction, but 14 in the y -direction.

This finite-helical-strip texture maintains until B_z is increased to 0.35 T. When $B_z = 0.36$ T, four skyrmions are observed at $T/\mathcal{J} = 1.9, 1.8,$ and 1.7 inside the square lattice. However, the skyrmions are not evenly distributed, since now the 30×30 square lattice does not fit the periodical textures even if they exist in reality. Nevertheless, as temperature T/\mathcal{J} falls down below 1.6, the magnetic system re-assumes its finite-helical-strip texture again. These strips can be classified into two groups which are orthogonal to each other as observed in experiment [10]. Now λ is about 14 in either x or y direction, which mismatches with the lattice size, so that the calculated spin configuration does not look very symmetric. Therefore, to obtain accurate calculated results, we must adjust the lattice size to find the best one which has the lowest total (free) energy.

While B_z is further increased, the spin textures consisting of sparse deformed skyrmions and vortices can be observed, but they are quite irregular,

probably for the sake just described. *These spin textures resemble those depicted in Figure 3(g) of Ref.[10].*

Finally, as $B_z \geq 0.86$ T, all spins are rotated by the external magnetic field to the z -direction, the whole system is polarized to be completely ferromagnetic.

3.8. Phase Diagram, Winding Numbers and Helicities of Spin Textures

The main part of the phase diagram in the low temperature range is displayed in Figure 7(a) for the 2D magnetic system. As the magnetic field strength falls in the region 0.11 T $\leq B \leq 0.27$ T, SkX textures are induced. Below this phase, as $B \leq 0.10$ T, helical strips are formed, except the cases when $B = 0.10$, SkX texture appears at $T/\mathcal{J}=0.32$, then it is greatly stretched along the $[-110]$ direction at $T/\mathcal{J} = 0.31$. And in a field range 0.29 T $\leq B \leq 0.35$ T, the helix plus skyrmion textures emerge above the SkX phase. Naturally, in a strong magnetic field, the whole system becomes completely ferromagnetic.

This phase diagram resembles qualitatively that observed in experiment [10]. Since our used model has been scaled and the system is simplified to be ideal, disparity with experiment is inevitable. Comparing the phase diagrams got numerically by means of our quantum approach and the CMC method [10], we find that the thermal spin fluctuations have been considerably overestimated in CMC simulation, but underestimated in our computation. The disparity arisen from our method is due to the molecular-field theory that has been implemented in the computing program. But this difficulty can be easily overcome by introducing randomly fluctuating terms or factors in the effective magnetic field.

With Eq.(7,8) given in Sec.II, the sums of the winding number density, $\sum_i \rho_i$, over the whole lattice and the averaged helicities per site γ for the spin textures are calculated, the corresponding curves are displayed in Figure 7(b,c).

As shown in above figures, in one SkX, a skyrmion is usually surrounded by four shallow unfully developed and frequently considerably deformed vor-

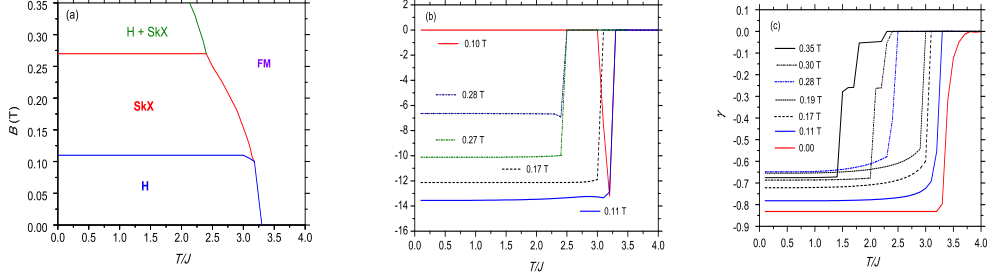


Figure 7. (a) Phase diagram of the magnetic system, (b) total winding number, and (c) helicity curves of the spin textures in external magnetic fields of different strengths.

B_z (T)	0.11	0.13	0.15	0.17	0.19	0.23	0.27
N_s	18	18	18	15	12	12	12
Q_{av}	-0.753	-0.770	-0.771	-0.809	-0.845	-0.845	-0.843

Table 1: Averaged winding numbers per *skyrmion complex* calculated at $T/\mathcal{J} = 0.1$ within external magnetic field of different strengths.

tices of appreciable sizes. These skyrmions and their neighboring vortices are entangled together, so that it is very difficult to identify the boundaries between these two sorts of chiral spin textures. For such a SkX, the averaged winding number Q_{av} per spin complex, consisting of one skyrmion and the parts of its neighboring vortices, can be estimated by dividing the sum, $\sum_i \rho_i$, with the skyrmion number N_s observed inside the 30×30 square lattice. Table 1 lists these averaged numbers obtained at $T/\mathcal{J} = 0.1$ in external magnetic fields of different strengths. We know already that as B_z changes from 0.11 to 0.27 T, N_s decreases from 18 to 12, so Q_{av} is expected to change accordingly.

In the absence of external magnetic field, the helical structure is the ground state of the system, no skyrmion is formed, so $\sum_i \rho_i = 0$, and the helicity per spin $\gamma = -0.831$ while $T/\mathcal{J} \leq 3.2$.

When $B_z = 0.10$ T, the system behaves extremely unusually. In the

temperature region $T/\mathcal{J} \leq 3.0$, $\sum_i \rho_i$ is always equal to zero, that is, no skyrmion can be formed and the helical texture dominates. However, at $T/\mathcal{J} = 3.2$, $\sum_i \rho_i$ suddenly falls down to -13.201 ($Q_{av} = -0.7334$) where SkX emerges, then immediately increases to -7.568 ($Q_{av} = -0.420$) at $T/\mathcal{J} = 3.1$ where the SkX is considerably deformed as shown in Figure 2.

While $B_z = 0.28$ T and $T/\mathcal{J} = 2.4$, eight skyrmions are observed. But below this temperature, four skyrmions and four bimerons appear. If one bimeron is considered to be composed of two semi-skyrmions, so the total skyrmion number shown in Figure 6(b) is approximately eight, which gives $Q_{av} = -0.830$ for one skyrmion complex, that is close to those values tabulated in Table 1.

More interestingly, the topological charge density calculated with Eq.(7) for every SkX also forms periodical and symmetric lattice which looks almost identical to the corresponding magnetic SkX, as displayed in Figure S1 of the supplementary part, demonstrating the correctness of our simulations.

Obviously, when the system is polarized by a strong external magnetic field to become completely ferromagnetic, the averaged helicity per site γ is equal to zero as shown in Figure 7(c). In the helical state, γ is around -0.8313, and in the case of SkX texture, the helicity is found to be in the region $-0.7822 < \gamma < -0.4072$. The points with $\gamma = 0$ form the boundary between the ferromagnetic and chiral phases.

4. Conclusions and Discussion

We have employed a quantum simulation approach to investigate a quasi-2D $\text{Fe}_{0.5}\text{Co}_{0.5}\text{Si}$ -like ferromagnetic system. In the absence of external magnetic field, the helical texture is the ground state. When a moderate external magnetic field is exerted perpendicular to the monolayer, SkX textures of the HCP structure are induced. As the magnetic field strength is increased, the SkX textures can be deformed, rotated, and the periodical lengths increased. Afterwards, complicated spin structures, such as skyrmions plus bimerons,

finite-length helical strips, sparse skyrmions surrounded by vortices, appear successively. And finally, the system becomes ferromagnetic as $B_z \geq 0.86$ T.

In each SkX, the spins of a skyrmions align clockwise in the xy -plane, while those of the neighboring shallow vortices order anti-clockwise in the same plane, so that the total (free) energy of the whole system can be minimized and the SkX texture stabilized. All chiral spin textures are right-handed since D is positives. Moreover, the calculated topological charge density for every SkX also forms periodical and symmetric lattice which is almost identical to the corresponding SkX, demonstrating the correctness of our simulations.

In a zero or weak magnetic field, the periodic wavelengths of the helical and SkX textures agree roughly with the theoretical values estimated with Eq.(6). Late on, we found that [32], when a weak a magnetic field is applied, another formula

$$\tan\left(\frac{2\pi}{\lambda}\right) = \frac{D}{\mathcal{J}} \quad (9)$$

agrees better with the SkX periodicity in the diagonal [110] or [-110] direction, as shown in Figure 2. However, this formula was actually derived for the helical state based on a continuous model [34]. As indicated by the authors, for the skyrmion states, no analytical expression for the periodicity can be obtained [34]. Nevertheless, if the wavelength estimated from Eq.(6) is projected onto the diagonal direction, it gives a value that is roughly equal to the periodicity evaluated from Eq.(9).

As B_z is enhanced, the periodicity is increased. Consequently, the lattice size chosen for simulation cannot fit the spin texture any longer, this mismatch can destroy the periodical structures in simulations even they exist in reality. Therefore, in order to generate symmetric and periodic spin textures and to study the physical properties accurately in strong external magnetic field, the lattice size has to be adjusted. In principle, a lattice which gives the lowest total (free) energy is expected to produce the best results.

An isolated skyrmion can be induced from the helical state when the external magnetic field is stronger than the critical value $B_{c1} = 0.2D^2/\mathcal{J}$ [35, 36, 42]. Inserting the values of \mathcal{J} and D we use here into this formulae

provides $B_{c1} = 0.148$ T, which is comparable to $B_{c1} = 0.11$ T that we find in our simulations. On the other hand, if B exceeds another critical value $B_{c2} = 0.8D^2/\mathcal{J}$, SkX texture disappears, the skyrmion plus bimeron states emerge afterwards [35, 36, 42]. The above two formulas gives the ratio $B_{c1}/B_{c2} = 0.25$. However, for FeGe and $\text{Fe}_{0.5}\text{Co}_{0.5}\text{Si}$, the ratios of the two transition fields are observed in experiments to be within a range of (0.3, 0.39). In the present case, we find in simulations that $B_{c2} = 0.28$ T, the ratio B_{c1}/B_{c2} is approximately 0.39, which agrees well with the experimental observation.

In chiral magnetic systems, the SkX wavelengths are usually quite large. To calculate and display their periodical spin textures, the grid model has to be used, where \mathcal{J} and D parameters are scaled, so are other physical quantities [35, 36]. To do this, we further quantize the grid with a quantum spin. From the calculated results presented above, we can conclude that this treatment is quite effective in describing the detailed spin textures of the quasi-2D system, as they evolve, driven by changing temperature and external magnetic field.

Especially, the skyrmions recently observed at interfaces are only a few nanometers in diameter [17, 25, 26, 35], and it is these magnetic materials that are of great importance in future technology. Obviously, within these magnetic systems, the spin vectors cannot change continuously, thus our discrete quantum model is expected to be more accurate and effective than those popularly used classical ones.

Acknowledgement

Z.-S. Liu acknowledges the financial support provided by National Natural Science Foundation of China under grant No. 11274177 and by University of Macau. H. Ian is supported by FDCT of Macau under grant 065/2016/A2 and by National Science Foundation of China under grant 11404415.

References

- [1] A. N. Bogdanov and U. K. Rößler, *Phys. Rev. Lett.* 87 (2001) 037203.
- [2] M. Lee, W. Kang, Y. Onose, Y. Tokura, and N.P. Ong, *Phys. Rev. Lett.* 102 (2009) 186601.
- [3] T. Schulz, R. Ritz, A. Bauer, M. Halder, M. Wagner, C. Franz, C. Pfeiderer, K. Everschor, M. Garst, and Rosch A, *Nat. Phys.* 8 (2012) 301.
- [4] J. F. Jonietz, S. Mhlbauer, C. Pfeiderer, A. Neubauer, W. Mnzer, A. Bauer, T. Adams, R. Georgii, P. Böni, R. A. Duine, K. Everschor, M. Garst, and A. Rosch, *Science* 330 (2010) 1648.
- [5] T. Skyrme, *Nucl. Phys.* 31 (1962) 556.
- [6] A. Bogdanov, and D. A. Yablonskii, *Sov. Phys. JETP* 68 (1989) 101
- [7] A. Bogdanov, and A. Hubert, *J. Mag. Mag. Mat.* 138 (1994) 255.
- [8] C. Pappas, E. Lelièvre-Berna, P. Falus, P. M. Bentley, E. Moskvina, S. Grigoriev, P. Fouquet, and B. Farago, *Phys. Rev. Lett.* 102 (2009) 197202.
- [9] S. Mühlbauer, B. Binz, F. Jonietz, C. Pfeiderer, A. Rosch, A. Neubauer, R. Georgii, and P. Böni, *Science* 323 (2009) 915.
- [10] X. Z. Yu, Y. Onose, N. Kanazawa, J. H. Park, J. H. Han, Y. Matsui, N. Nagaosa, and Y. Tokura, *Nature* 465 (2010) 901904.
- [11] X. Z. Yu, N. Kanazawa, Y. Onose, K. Kimoto, W. Z. Zhang, S. Ishiwata, Y. Matsui, and Y. Tokura, *Nat. Mater.* 10 (2011) 106.
- [12] A. Crépieux, and C. Lacroix, *J. Mag. Mag. Mat.* 182 (1998) 341.

- [13] M. Bode, M. Heide, K. von Bergmann, P. Ferriani, S. Heinze, G. Bihlmayer, A. Kubetzka, O. Pietzsch, S. Blügel, and R. Wiesendanger, *Nature* 447 (2007) 190.
- [14] S. Heinze, K. von Bergmann, M. Menzel, J. Brede, A. Kubetzka, R. Wiesendanger, G. Bihlmayer, and S. Blügel, *Nat. Phys.* 7 (2011) 713.
- [15] N. Romming, C. Hanneken, M. Menzel, J. E. Bickel, B. Wolter, K. von Bergmann, A. Kubetzka, and R. Wiesendanger, *Science* 341 (2013) 636.
- [16] B. Dupé, M. Hoffmann, C. Paillard, S. Heinze, *Nat. Commun.* 5 (2014) 4030.
- [17] B. Dupé, G. Bihlmayer, S. Blügel, and S. Heinze, *Nat. Commun.* 7 (2016) 11779.
- [18] S. Seki, X. Z. Yu, S. Ishiwata, and Y. Tokura, *Science* 336 (2012) 198.
- [19] T. Moriya, *Phys. Rev.* 120 (1960) 91.
- [20] I. E. Dzyaloshinskii, *Sov. Phys. JETP* 5 (1957) 1259.
- [21] A. Fert, V. Cros, and J. Sampaio, *Nat. Nanotech.* 8 (2013) 152.
- [22] J. Sampaio, V. Cros, S. Rohart, A. Thiaville, and A. Fert, *Nat. Nanotech.* 8 (2013) 839844.
- [23] J. H. Han, J. Zang, Z. Yang, J.-H. Park, and N. Nagaosa, *Phys. Rev. B* 82 (2010) 094429.
- [24] Magnetic skyrmion, https://en.wikipedia.org/wiki/Magnetic_skyrmion
- [25] J. Hagemeister, D. Iaia, E. Y. Vedmedenko, K. von Bergmann, A. Kubetzka, and R. Wiesendanger, *Phys. Rev. Lett.* 117 (2016) 207202.
- [26] J. Hagemeister, N. Romming, K. von Bergmann, E.Y. Vedmedenko, R. Wiesendanger, *Nat. Commun.* 6 (2015) 8455.

- [27] Z.-S. Liu, V. Sechovský, M. Diviš, J. Phys.: Condens. Matter 23 (2011) 016002.
- [28] Z.-S. Liu, V. Sechovský, M. Diviš, Phys. Status Solidi B 249 (2012) 202.
- [29] Z.-S. Liu, H. Ian, J. Nanopart. Res. 18 (2016) 9.
- [30] Z.-S. Liu, O. Ciftja, H. Ian, Physica E 90 (2017) 13.
- [31] Z.-S. Liu, O. Ciftja, X.-C. Zhang, Y. Zhou, H. Ian, Superlatt. Microstruct. 117 (2018) 495.
- [32] Z.-S. Liu, H. Ian, J. Phys. Condens. Matter. 18 (2019) 215302.
- [33] Z.-S. Liu, H. Ian, *Superlatt. Microstruct.* 126 (2019) 25.
- [34] A. O. Leonov, T. L. Monchesky, N. Romming, A. Kubetzka, A. N. Bogdanov, and R. Wiesendanger, New J. Phys. 18 (2016) 065003.
- [35] H. Y. Kwon, S. P. Kang, Y. Z. Wu, and C. Won, J. Appl. Phys. 113 (2013) 133911.
- [36] H.Y. Kwon, K.M. Bu, Y.Z Wu, C.Won, J. Magn. Mater. 324 (2012) 2171.
- [37] J. P. Chen, D.-W. Zhang, J.-M. Liu, Sci. Rep. 6 (2016) 29126.
- [38] K. Shibata, X. Z. Yu, T. Hara, D. Morikawa, N. Kanazawa, K. Kimoto, S. Ishiwata, Y. Matsui, and Y. Tokura Nat. Nanotech. 8 (2013) 723.
- [39] W. T. Hou, J. X. Yu, M. Daly, and J. D Zang, Phys. Rev. B 96 (2017) 140403(R).
- [40] M. Ezawa, Phys. Rev. Lett. 105, 197202 (2010) 197202.
- [41] M. Ezawa, Phys. Rev. B 83 (2001) 100408(R).
- [42] J. H. Han, J.D. Zang, Z.H. Yang, J.H. Park, and N. Nagaosa, Phys. Rev. B 82 (2010) 094429.